Phase behaviour of heteronuclear dimers in three-dimensional systems—a Monte Carlo study

2008 J. Phys.: Condens. Matter 20 415101

(http://iopscience.iop.org/0953-8984/20/41/415101)

J. Phys.: Condens. Matter **20** (2008) 415101 (9pp) doi:10.1088/0953-8984/20/41/415101

Phase behaviour of heteronuclear dimers in three-dimensional systems—a Monte Carlo study

W Rżysko[1] **and K Binder**[2]

[1] Faculty of Chemistry, MCS University, 20031 Lublin, Poland
[2] Institute für Physik, Johannes Gutenberg-Universität, 55099 Mainz, Germany

E-mail: wojtekrzysko@gmail.com

Received 2 April 2008, in final form 24 July 2008
Published 5 September 2008
Online at stacks.iop.org/JPhysCM/20/415101

Abstract
Monte Carlo simulation in the grand canonical ensemble, the histogram reweighting technique and finite size scaling are used to study the phase behaviour of dimers in three-dimensional systems. A single molecule is composed of two segments A and B, and the bond between them cannot be broken. The phase diagrams have been estimated for a set of model systems. Different structures formed by heteronuclear dimers have been found. The results show a great variety of vapour–liquid coexistence behaviour depending on the strength of the interactions between segments.

1. Introduction

One of the most interesting problems in the theory of fluids is their phase behaviour. In particular, phase transitions in single-component fluids have been a subject of abiding interest to theorists for many years. In the simplest model of fluids a molecule is treated as a point source of a spherically symmetrical intermolecular potential. Such a molecule has only translational degrees of freedom. The molecules do not exhibit any anisotropic features such as magnetic moment or electric charge. The isotropic intermolecular interactions can be separated into a repulsive part and an attractive part. The range and strength of these interactions significantly affect phase transitions in the systems [1–4]. Much more complex phase behaviour was found for fluids in which a particle carries an internal degree of freedom, as for instance a magnetic moment, a spin or a dipolar moment. In this case fluids exhibit additional phase transitions associated with internal degree of freedom, e.g. a transition between ferromagnetic and paramagnetic fluids [5] or a transition between isotropic and ferroelectric fluids [6]. Studies have considered various lattice-based [7, 8] as well as continuum fluid models [9–13].

Various methods of statistical mechanics have been used to deal with such models. Mean-field analysis and density functional theory have been applied to describe a dipolar fluid [5, 9] and a Heisenberg spin fluid [6, 12, 13]. Computer simulations have been performed for a two-dimensional spin fluid [14], a three-dimensional Heisenberg fluid [11, 15], a spin $1/2$ quantum fluid [16] and a van der Waals–Potts fluid [10]. The phase diagrams obtained for these models showed unusual richness of phases stemming from competition between different forces. For some single-component fluids with internal degrees of freedom the topology of phase diagrams is analogous to that observed in apparently distinct systems, such as binary liquid mixtures [17] or ionic fluids [18, 19]. This observation is at first sight surprising, but can be easily explained because one can consider these systems as fluids consisting of molecules having two-state internal degrees of freedom. In the case of a binary mixture the particle species can be interpreted as a kind of 'pseudospin' variable [17].

Another group of fluid models explicitly involve the architecture of molecules and mimic their shape and chemical composition. A molecule can be modelled as a complex structure built of the same or different units (segments) linked together. Such a model is often used to describe normal and branched polymeric chains. The energy of interaction between two molecules is the sum of segment–segment interactions. In other words, the potential acting between a pair of chains is a multicentre one. The simplest molecule of this sort is a dimer. In this paper we deal with the phase behaviour of a special class of dimers.

For many years systems involving dimers have been studied in the framework of both lattice and off-lattice models [20–38]. In lattice-based theories multisite occupancy

models are implemented and each unit of the molecule occupies different lattice sites. In theoretical studies the key problem is to estimate a number of possible configurations for the system. This task is much more difficult than for the single-site problem because there is no statistical equivalence between molecules and vacancies. If a given lattice site is occupied by a dimer segment then at least one of nearest-neighbour sites is also occupied. To date much effort has been devoted to estimating the number of configurations. The exact solution of this problem is known only for homogeneous dimers in the two-dimensional system at full surface coverage [22–24]. Other studies have been devoted to homogeneous dimers. Dimers built from different segments have been less intensively studied [32–38]. A heterogeneous dimer is a model of diatomic molecules, e.g. CO or NO. On the other hand, a heterogeneous dimer can mimic a molecule consisting of two considerably different parts. One can mention here such chemical compounds as alcohols, amines and amphiphiles. Molecules of amphiphiles contain both hydrophilic and hydrophobic parts. The difference in properties of both parts is the most important reason for the self-assembly and the existence of various phases in amphiphilic systems [39]. Adsorption of dimers has been explored using theoretical and experimental methods [40–43]. The orientation of CO molecules adsorbed on Mg(100) crystalline surfaces and on alkali halides with the rocksalt structure was studied by using spectroscopic analysis [44] and quantum calculations [43]. The experiments showed that, depending on the conditions, dimers can be perpendicular or parallel to the surface; moreover, different ordered structures were found in such monolayer films. The systems consisting of heterogeneous dimers exhibit a great variety of phase transitions. In our previous papers we dealt with phase behaviour of the dimers in two-dimensional systems [32–38]. Two-dimensional systems can mirror the properties of monolayers formed by adsorption on flat surfaces or in very narrow pores. It is well known that space dimensionality has an important effect on the phase behaviour. This fact is one reason for extending our studies to three-dimensional systems containing dimers. Moreover, a description of interfacial systems requires knowledge of properties of the bulk fluids. Lattice-based theories are often used to describe molecular fluids in various systems, so it is important to analyse possible phase transitions occurring for such models. In this paper we explore the phase behaviour of heteronuclear dimers in a three-dimensional lattice system using Monte Carlo simulation methods.

The main aim of this work is to understand how the topology of the phase diagram depends upon the relative strength of interaction between segments.

2. The model

We consider a three-dimensional system consisting of N heterogeneous dimers built from the segments A and B. We introduce a lattice model with a site occupied by one segment. A pair of occupation variables (cA, cB) characterizes each lattice site; cx (x denotes a kind of the segment) can take the values $cx_i = 1$ when a site is occupied by the segment x and $cx_i = 0$ in other cases. Only the nearest-neighbour interactions are taken into account. In the grand canonical ensemble the Hamiltonian has the following form:

$$\mathcal{H} = u_{AA}\sum_{\langle i,j\rangle} cA_i cA_j + u_{BB}\sum_{\langle i,j\rangle} cB_i cB_j + u_{AB}\sum_{\langle i,j\rangle} cA_i cB_j - Nu_{AB} - N\mu, \tag{1}$$

where μ is the chemical potential of dimers and u_{AA}, u_{BB} and u_{AB} are the energies of interactions for different pairs of segments. The summations labelled $\langle i, j\rangle$ are over all pairs of nearest-neighbour segments (including interactions between segments belonging to the same molecule). The term $(-Nu_{AB})$ is a correction following from the existence of bonds.

We introduce the spin variables in the following form:

$$S_i = \begin{cases} 1 & \text{for } cA_i = 1, \quad cB_i = 0 \\ 0 & \text{for } cA_i = 0, \quad cB_i = 0 \\ -1 & \text{for } cA_i = 0, \quad cB_i = 1. \end{cases} \tag{2}$$

Using a simple variable transformation

$$cA_i = S_i(S_i + 1)/2 \qquad cB_i = S_i(S_i - 1)/2 \tag{3}$$

one can rewrite the Hamiltonian (1) in the form of a spin-1 lattice model Hamiltonian:

$$\mathcal{H} = \epsilon\sum_{\langle i,j\rangle} S_i^2 S_j^2 + \epsilon_1\sum_{\langle i,j\rangle} S_i S_j + \epsilon_2\sum_{\langle i,j\rangle}(S_i^2 S_j + S_i S_j^2) + H\sum_j S_j^2, \tag{4}$$

where the last sum is over all lattice sites, and

$$\epsilon = \tfrac{1}{4}(u_{AA} + u_{BB} + 2u_{AB}), \tag{5}$$

$$\epsilon_1 = \tfrac{1}{4}(u_{AA} + u_{BB} - 2u_{AB}), \tag{6}$$

$$\epsilon_2 = \tfrac{1}{4}(u_{AA} - u_{BB}), \tag{7}$$

$$H = \tfrac{1}{2}(u_{AB} - \mu). \tag{8}$$

When H is replaced by $H' = -\frac{1}{2}(\mu_A - \mu_B)$ the Hamiltonian (4) describes an equimolar binary mixture of monomers A and B. Depending on the relations between energy parameters, the Hamiltonian (4) describes different models. For symmetrical segment–segment interactions ($u_{AA} = u_{BB}, \epsilon_2 = 0$) the Hamiltonian (4) corresponds to the Blume–Emery–Griffiths [45] model. When, additionally, $\epsilon = 0$, the Hamiltonian is appropriate for the Blume–Capel model [46, 47]. A two-dimensional fluid of heterogeneous dimers with symmetrical, attractive interactions ($\epsilon_2 = 0, \epsilon, \epsilon_1 < 0$) has been discussed in [32]. However, when $u_{AB} = u_{BB}$(then $\epsilon_1 = \epsilon_2$) the Hamiltonian (4) can be rewritten as

$$\mathcal{H} = \epsilon\sum_{\langle i,j\rangle} S_i^2 S_j^2 + \epsilon_1\sum_{\langle i,j\rangle} S_i S_j(S_i + S_j + 1) + H\sum_j S_j^2. \tag{9}$$

The phase behaviour of such a class of dimers in two-dimensional systems was studied in [33–35] and the ground

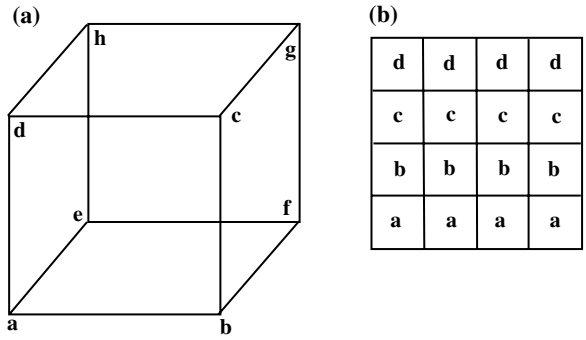

Figure 1. Schematic representation of the sublattices used to calculate the order parameters for the AF (a) and SAF (b) phases.

state for the Hamiltonian (4) was discussed in [35]. For $\epsilon < 0$ all possible ordered states correspond to a completely covered lattice. When $\epsilon > 0$ the ordered structures can also be formed at lower densities [30, 31]. For $\epsilon_1 < 0$ the mixed pairs AB are energetically profitable and the antiferromagnetic structure of segments (AF) is stable. The bonds are randomly distributed over the lattice. When $\epsilon_1 = 0$ a completely disordered phase is observed. However, for $\epsilon_1 > 0$ the contacts AA and BB are preferred and the super-antiferromagnetic phase (SAF (4×1)) structure is formed. The structure consists of replicated $AABB$ layers in which all bonds are parallel. One can say that there is an ordering of segments as well as an ordering of bonds. This structural transition is to some degree similar to demixing in a binary mixture of monomers A and B [17]. In the considered case, however, the segments A and B are permanently bonded so differences in strengths of interactions between the same and different segments can only cause change in the orientation of molecules.

In three-dimensional systems the order parameters for these structures can be defined as follows. In the case of the AF structure we use the parameter

$$\psi_{\mathrm{AF}} = m_a - m_b + m_c - m_d - m_e + m_f - m_g + m_h, \quad (10)$$

where

$$m_i = \frac{1}{L^3} \sum_{(i \in k)} S_i, \quad (11)$$

and where k denotes the sublattice a, b, c, d, f, g, h defined in figure 1(a), L is the linear size of the system. For a perfect phase AF $|\psi_{\mathrm{AF}}| = 1$. Note that the AF-phase is characterized by an one-component order parameter.

The order parameter for the SAF (4×1) structure can be expressed as

$$\psi_{\mathrm{2D,SAF}} = \sqrt{\psi_{1,x}^2 + \psi_{2,x}^2 + \psi_{1,y}^2 + \psi_{2,y}^2}, \quad (12)$$

and

$$\psi_{\mathrm{SAF}} = \sqrt{\psi_{1,x}^2 + \psi_{2,x}^2 + \psi_{1,y}^2 + \psi_{2,y}^2 + \psi_{1,z}^2 + \psi_{2,z}^2}. \quad (13)$$

where

$$\psi_{1,\alpha} = m_a + m_b - m_c - m_d, \quad (14)$$

$$\psi_{2,\alpha} = m_a - m_b - m_c + m_d, \quad (15)$$

for $\alpha = x,\ y,\ z$.

The sublattice a, b, c, d is defined in figure 1(b) for a perfect SAF-phase $\psi_{\mathrm{SAF}} = 1$.

To study the liquid–vapour transition we use the usual order parameter defined as

$$m = \rho - \langle \rho \rangle, \quad (16)$$

where

$$\rho = \frac{1}{L^3} \langle S_i^2 \rangle. \quad (17)$$

In general, for a system which does not exhibit the special symmetry of the order parameter (as the magnetization in the Ising model) the field-mixing effects should be taken into account [48] and the order parameter is expressed as a linear combination of the density and energy. However, many authors have used the order parameter m to estimate the critical parameters and obtained sufficiently accurate results [49, 50].

3. Monte Carlo simulation

All simulation techniques used in our study have been described elsewhere [51–55], therefore we confine the discussion of the methodology to the most important aspects. The simulations were conducted in the grand canonical ensemble using hyper-parallel tempering [54]. The cubic simulation cell was used with the standard periodic boundary conditions in all (x, y, z) directions. The linear dimension of the system ranges between $L = 12$ and $L = 40$. The Monte Carlo step (MCS) consisted of an attempt to insert a molecule at a randomly chosen position with random orientation, or an attempt to remove an existing particle. A typical equilibration run consisted of 10^6 MCS (per site) and the production run amounted to about 10^8 MCS. We have calculated the density, the order parameters and the average energy (u). In our work we use $|u_{BB}|$ as the unit of the energy.

Multiple-histogram reweighting was applied to analyse the results [55, 56]. We collected the histograms of density $P(\rho)$ and suitable order parameters $(P(\psi))$ for systems of different sizes. In finite systems close to a phase coexistence the density distributions $P(\rho) = \int P(\rho, u)\mathrm{d}u$ has two peaks. The vapour–liquid coexistence curves have been determined according to the equal area rule, i.e. by tuning the chemical potential at a given temperature until the areas under two peaks in the density distribution $P(\rho)$ become the same [55].

The ordering in the system was detected by means of the order parameters m, ψ_{AF} and ψ_{SAF}. These order parameters are complemented by corresponding susceptibilities

$$\chi_{\psi,L} = \frac{1}{kT} [\langle \psi^2 \rangle - \langle |\psi| \rangle^2] \quad (18)$$

and the fourth-order cumulants [57]

$$U_{\psi,L} = 1 - \frac{\langle \psi^4 \rangle}{3 \langle \psi^2 \rangle^2}. \quad (19)$$

In the case of a first-order transition the maximum value of susceptibility scales with the system size as [58–60]

$$\chi_{\max,L} \propto \chi_0 + \alpha L^D, \quad (20)$$

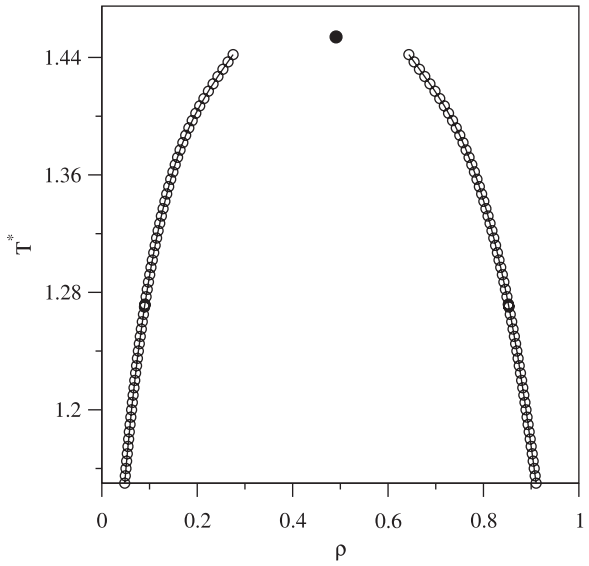

Figure 2. Phase diagram in the T–ρ plane for $u_{AA} = u_{BB} = u_{AB} = -1$ and $L = 12$.

where $\chi_0 = (\chi^+ + \chi^-)/2$, χ^+ and χ^- are the values of the susceptibility in the two coexisting phases at the transition point, D is the system dimensionality and α is a constant. Thus

$$\chi_{\mathrm{corr,L}} \propto \alpha L^D, \tag{21}$$

where $\chi_{\mathrm{corr}}(L) = \chi_{\mathrm{max}}(L) - \chi_0$. The values of χ_0 can be estimated from the plot of $\chi_{\mathrm{max}}(L)$ versus L^D, by extrapolating the data to $L = 0$.

According to the finite size scaling theory the order–disorder transition in a finite system is rounded and shifted. For this reason the transition parameters have been determined from the well-known scaling relationships [53]. The true transition temperature was extracted from the plot $U_{\psi,L}$ versus T ($U_{\psi,L}$ versus μ) obtained for various values of L, since all the curves intersect at $T(\mu)$ giving the fixed value U^*_ψ. The value U^*_ψ characterizes the universality class of the transition.

4. Results and discussion

4.1. Homogeneous dimers

We begin with the presentation of the phase diagram estimated for homogeneous dimers on a three-dimensional cubic lattice (figure 2). The universal value of U^*_{m} extracted from the cumulant crossings point equals 0.47 (see figure 3(d)). Note that Ferrenberg and Landau obtained the same result for a three-dimensional simple cubic Ising model [61]. We obtained the following critical parameters for dimers: $T_{\mathrm{c}} = 1.454$, $\mu = -3.907$.

As we have already mentioned, our main goal is to study the phase behaviour of heterogeneous dimers. The effects of differences in the strength of interactions between segments on phase transitions in two-dimensional monolayers was discussed in our previous papers [32–36]. Below we

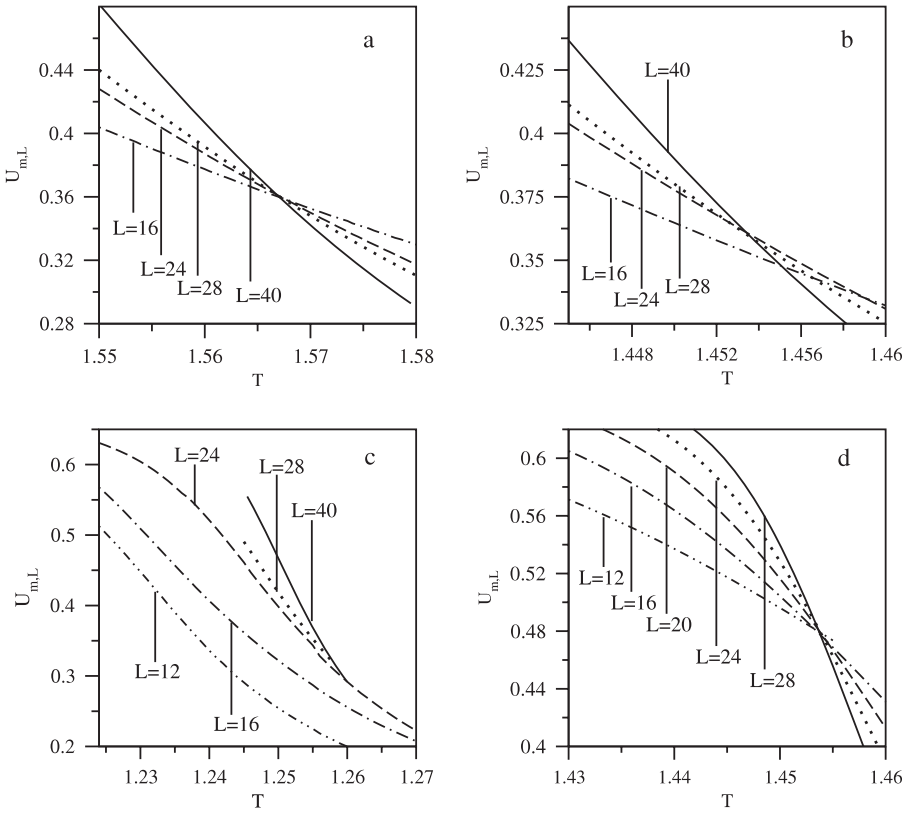

Figure 3. The changes of the fourth-order cumulants $U_{\mathrm{m},L}$ with temperature for systems characterized by $u_{BB} = u_{AB} = -1$, calculated along the coexistence curve for different sizes of the simulation cell L (given in the figure) for various values of u_{AA}: (a) $u_{AA} = 1$, (b) $u_{AA} = 0.5$, (c) $u_{AA} = 0$ and (d) $u_{AA} = -1$.

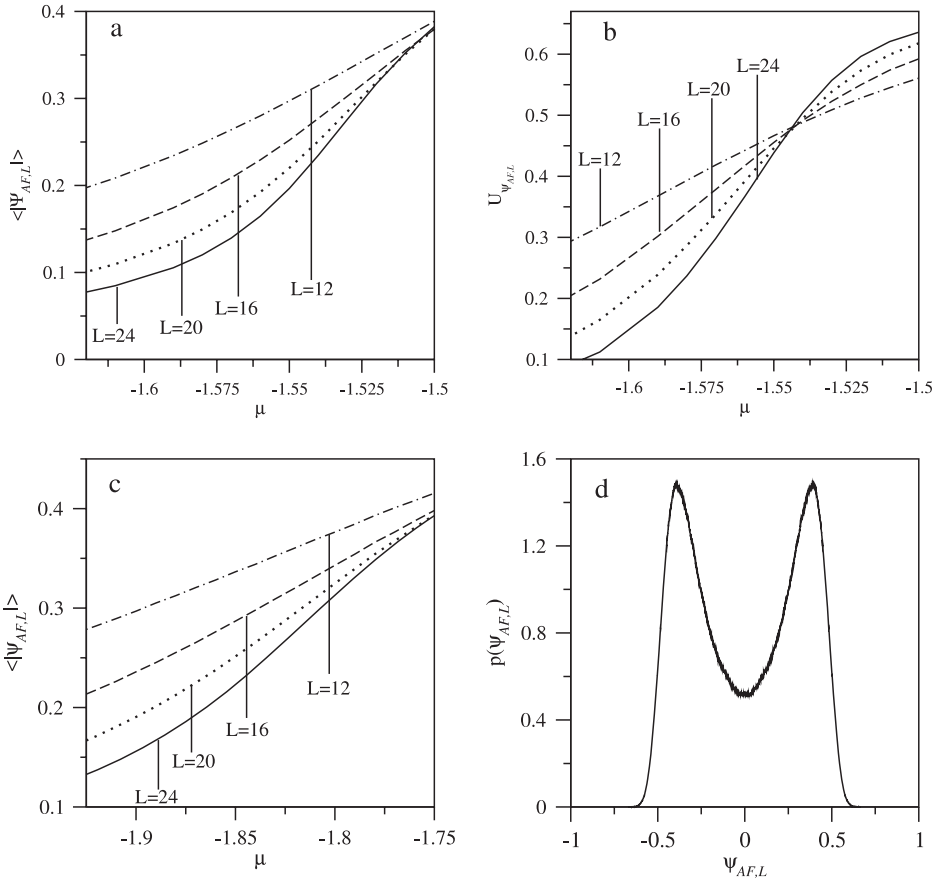

Figure 4. The dependences of the order parameter $|\psi_{\mathrm{AF},L}|$ (a) and its fourth-cumulant ($U_{\psi_{\mathrm{AF},L}}$) (b) on the chemical potential for $u_{BB} = u_{AB} = -1$, $u_{AA} = 1$ at $T = 1.9$ and different system sizes, given in the figure. Part (c) shows the changes of the order parameters $|\psi_{\mathrm{AF},L}|$ with the chemical potential for systems characterized by $u_{BB} = u_{AB} = -1$, $u_{AA} = 0$ at $T = 1.5$, obtained for different system sizes of the simulation cell (shown in the figure). Part (d) shows the distribution of the order parameter ψ_{AF} estimated at the maximum of susceptibility $\mu = -1.83$ at $T = 1.5$ for $L = 16$.

consider two classes of systems: systems with a stable AF-phase and system for which the SAF-phase is formed.

4.2. Heterogeneous dimers with a stable AF-phase

The results obtained for $u_{BB} = u_{AB} = -1$ and $u_{AA} \in [-1, 1]$ are shown in figures 3–7. In such systems, apart from the case of homogeneous dimers ($u_{AA} = -1$), the AF-structure is stable. The density cumulants $U_{\mathrm{m},L}$ along the vapour–liquid coexistence curve as functions of temperature for different lattice sizes are plotted in figure 3. According to the finite size scaling theory these curves should have one well-defined intersection point. Indeed, for $u_{AA} = 1$ and for $u_{AA} = -1$ the fixed points can be precisely estimated by cumulant crossings even for relatively small systems. For strong repulsive AA-interactions ($u_{AA} = 1$) we found $U^*_{\mathrm{m}} \approx 0.36$. This value seems to be close to that corresponding to the universality class of a three-dimensional tricritical point model [62–64]. For attractive interactions ($u_{AA} = -1$), however, we obtained $U^*_{\mathrm{m}} = 0.47$, which is characteristic of the three-dimensional Ising model universality class [61]. Similar crossover between the universality classes was found for heterogeneous dimers in two-dimensional systems [35]. When the energy u_{AA} increases, the value of U^*_{m} changes rapidly, but estimation of the crossover point is very difficult.

For u_{AA} close to the crossover point the cumulant crossing method can only be used for large systems. This is illustrated in figure 3. For $u_{AA} = 0.5$ the curves obtained for $L = 16, 24, 28, 40$ do not intersect at one point. The intersection point of the curves for the two large systems yields $U^* \approx 0.36$. However, the results obtained for $u_{AA} = 0$ suggest that we are close to the region of crossover between different universality classes. In the latter case the intersection point for $L = 28, 40$ gives $U^*_{\mathrm{m}} < 0.30$.

Figures 4(a) and (b) present the dependences of the order parameter $|\psi_{\mathrm{AF}}|$ and its fourth-order cumulant ($U_{\psi_{\mathrm{AF},L}}$) on the chemical potential for $u_{AA} = 1$ and for different system sizes. These results were obtained at $T = 1.9$. This temperature is considerably higher than the critical temperature of the vapour–liquid transition (see figure 3; $T_{\mathrm{c}} = 1.567$). The changes in the order parameter are typical for second-order phase transitions. This implies that there is a second-order transition between a disordered fluid and an ordered fluid of the AF-type. The same conclusion follows from figure 4(c), where the order parameters versus the chemical potential are plotted for $u_{AA} = 0$. The existence of an ordered structure in the system is confirmed by an analysis of the distribution of the order parameter estimated at the susceptibility maximum ($T = 1.5$, $\mu = -1.83$). The distribution presented in figure 4(d)

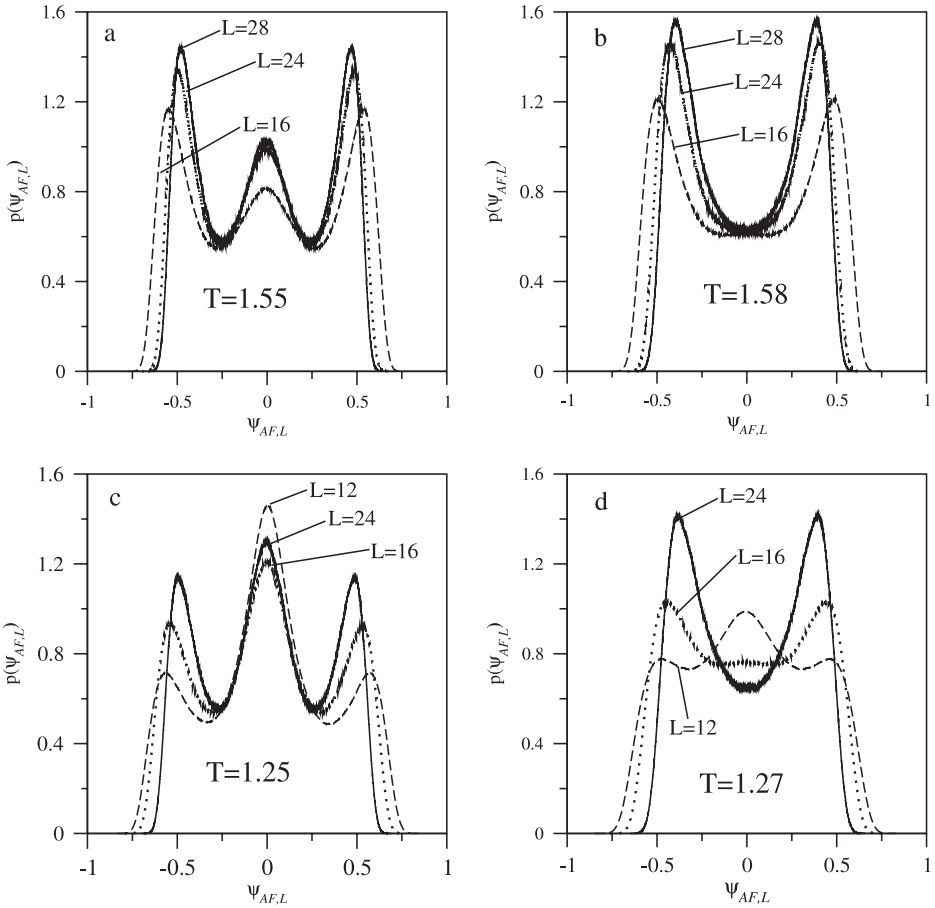

Figure 5. The distributions of the order parameter $\psi_{\mathrm{AF},L}$ for the systems characterized by $u_{BB} = u_{AB} = -1$, $u_{AA} = 1$ ((a), (b)) and $u_{BB} = u_{AB} = -1$, $u_{AA} = 0$ ((c), (d)), obtained for different sizes of simulation cell for selected temperatures (shown in figures), calculated along the coexistence curve.

possesses two symmetric maxima corresponding to the AF-structures. This distribution can be mapped into the master curve estimated with a high accuracy for the three-dimensional Ising model [65].

In figure 5 the distributions of the order parameter ψ_{AF} along the coexistence line are presented for different system sizes. The upper panels illustrate the structure of the system for $u_{AA} = 1$ and for two thermodynamic states (μ, T). At temperatures below the critical point of the condensation ($T = 1.55$) one can see two symmetric peaks corresponding to the ordered AF-liquid, and a middle, lower, peak corresponding to a disordered vapour. Above the critical temperature of the vapour–liquid transition (i.e. at $T = 1.58$) an ordered fluid is still observed, but only the ordered AF-phase is stable. In the lower panels the distributions for $u_{AA} = 0$ are depicted. At $T = 1.25$ the results are analogous to those obtained for $u_{AA} = 1$. However, in this case a change of the system size can qualitatively change the distribution. At $T = 1.27$ for small systems there is a maximum at $\psi_{\mathrm{AF}} = 0$ (a disordered phase), whereas for larger systems the minimum is observed. This is consistent with analysis of figures 3(b) and (c).

Figure 6 presents the phase diagrams estimated for $u_{AA} = 1$ and $u_{AA} = 0$. In the case of $u_{AA} = 1$ we found the λ-line corresponding to a second-order phase transition between a disordered and ordered AF-fluid, which meets the vapour–liquid coexistence curve at a critical point of condensation. Thus, the system possesses a tricritical point (marked by a black square). For $u_{AA} = 0$ we cannot judge whether the λ-line terminates at the critical point of condensation or at a critical end point.

We have supplemented our study with a series of simulations for the Hamiltonian corresponding to the Blume–Capel model ($\epsilon_1 = -J = -1$, $H = \mu$). The aim of these investigations was to estimate the universal value of U_{m}^* and the transition parameters for the tricritical point model in three dimensions. As follows from figure 7, the estimated cumulant is $U_{\mathrm{m}}^* \approx 0.352$. The critical temperature of condensation $T_{\mathrm{c}} = 1.393$ and the critical chemical potential $\mu_{\mathrm{c}} = -2.8488$. The value of U_{m}^* is somewhat lower than that obtained for dimers (see figure 3). However, it is well known that an accurate estimation of the critical parameters for systems exhibiting tricritical point behaviour is very difficult and different values are reported in the literature [62–64]. Note that $D = 3$ is the upper critical dimension for the tricritical point model. Bausch [66] showed that close enough to the tricritical point fluctuation effects dominate for $D < 3$ but for $D > 3$ the mean-field behaviour of the system was observed. This can explain numerical problems with estimation of critical parameters.

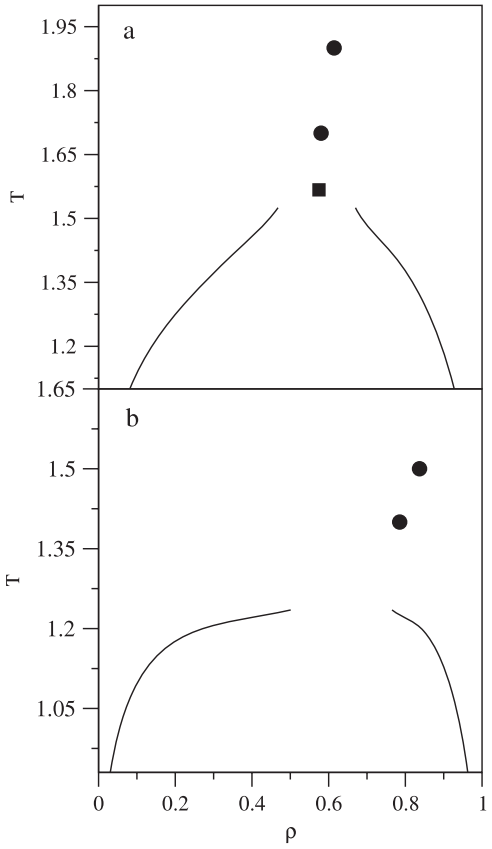

Figure 6. Phase diagrams in the T–ρ plane for the systems characterized by $u_{BB} = u_{AB} = -1$, for various values of the parameter u_{AA}: (a) $u_{AA} = 1$, (b) $u_{AA} = 0$.

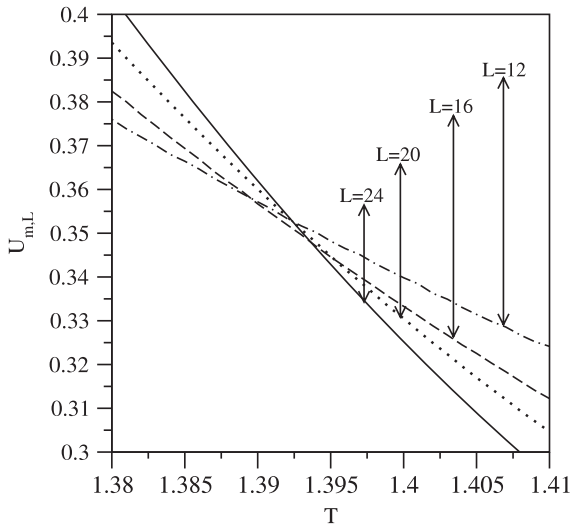

Figure 7. The cumulant intersection plot for the systems with different linear dimensions L for the Hamiltonian corresponding to Blume–Capel model.

4.3. Heterogeneous dimers with the stable SAF-phase

We turn now to the results for three-dimensional systems, in which stable SAF structures can be formed. We have considered attractive, symmetrical segment–segment

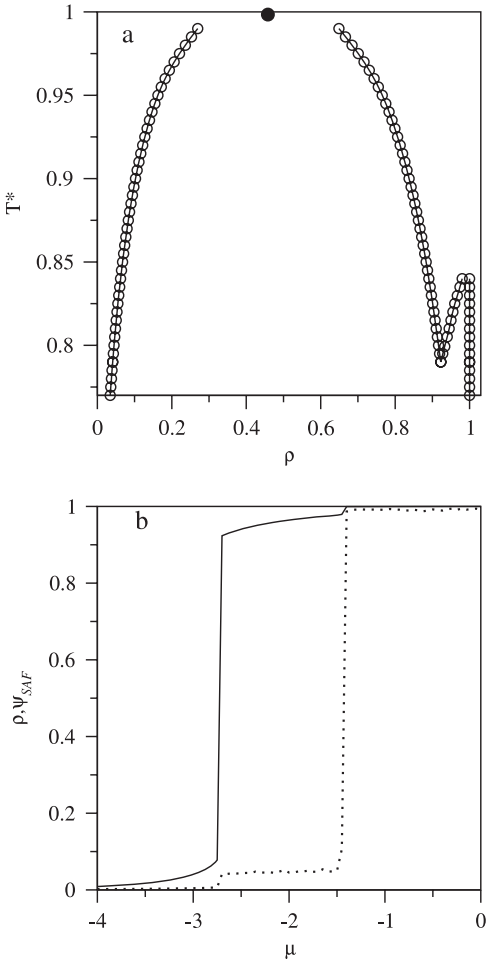

Figure 8. Phase diagram in the T–ρ plane for $u_{AA} = u_{BB} = -1$ and $u_{AB} = -025$ and $L = 12$ (a). The adsorption isotherm ρ (solid line) and order parameter ψ_{SAF} (dotted line) plotted for $u_{AA} = u_{BB} = -1$, and $u_{AB} = -0.25$ at $T = 0.825$ (b).

interactions, $u_{AA} = u_{BB} = -1$ and $u_{AB} = -0.25$. In this case the phase diagram splits into two parts corresponding to two first-order phase transitions. The first transition is the usual gas–liquid coexistence. The other one corresponds to the structural transition between two liquid phases—a disordered liquid and an ordered SAF-phase. Both branches join together in the triple point. The critical temperature of condensation on the cubic lattice, for this category of heterogeneous dimers, was estimated from an analysis of the density cumulants, $T_{\mathrm{c}} = 0.998$. The transition belongs to the universality class of the three-dimensional Ising model. When the energy of attraction decreases (u_{AB}) the triple point is shifted towards the critical point of condensation. For ($u_{AB} \approx 0$) there is only one phase transition between a disordered gas and an ordered liquid of the SAF type. The triple point disappears and the phase diagram is of the 'swan neck' type [32].

In the diagram presented in figure 8(a) two first-order transitions are visible: the first corresponds to vapour condensation whereas the second is the structural transition. In the range of temperatures [0.79, 0.84] two transitions are observed: the vapour–disordered liquid transition and the disordered liquid–ordered liquid transition. Below the triple

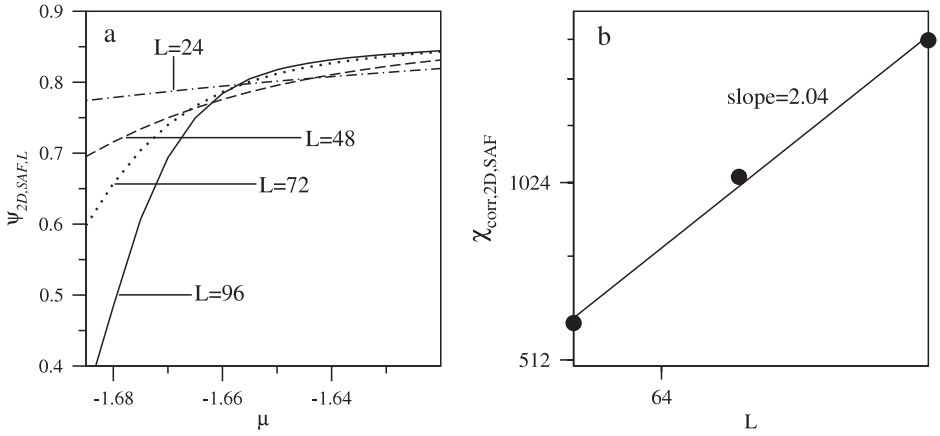

Figure 9. Changes of the order parameter $\psi_{2D,SAF}$ with the chemical potential for systems characterized by $u_{AA} = u_{BB} = -1$, $u_{AB} = -0.35$, calculated at the temperature $T = 0.515$ for different sizes of simulation cell given in the figure (a). Part (b) shows the log–log plot of the maximal susceptibility $\chi_{corr,SAF}$ on the system size.

point (around 0.79) only one transition, between the vapour and the ordered liquid, remains. Preliminary simulations have been performed for systems with $u_{AB} = 0$ and -0.125. Analysis of the isotherms and histograms leads to the following conclusions: for $u_{AB} = 0$ a 'swan neck' type phase diagram was found. The same class of phase diagram was observed for two-dimensional systems [32]. In the case of $u_{AB} = -0.125$ the phase diagram is similar to that presented in figure 8(a). The triple point is located at a higher temperature, $T \approx 0.825$, and the critical points for both transitions almost coincide. The triple point temperature decreases with the interaction energy u_{AB} approaching -1.

In figure 8(b) we present the density and order parameter ψ_{SAF} isotherms. The density isotherm exhibits two jumps, the first, larger, jump corresponds to the condensation, whereas the other, smaller, jump is connected to the structural transition. On the other hand, the order parameter isotherm exhibits one sharp jump at the chemical potential of the structural transition. Since 'the structural jump' on the density isotherm is small, the coexistence envelope between two stable liquids is very narrow. It is thus not clear whether the system really undergoes a first-order structural transition or, perhaps, one should expect a λ-line here. The structural transition occurs for systems with high densities, consequently the calculations require very long runs. The lattice is almost completely filled by dimers and any change of the system state is difficult. A similar phase diagram was estimated for dimers on a square lattice in two dimensions (figure 1 in [32]). Such simulations were considerably faster. Therefore we could consider bigger systems and achieve good statistics.

In order to resolve the question of the order of the structural transition in three dimensions we have performed additional calculations in two dimensions hoping that the conclusion will be similar. Figure 9(a) presents the dependences $\psi_{2D,SAF}$ versus μ for different system sizes in two dimensions. For large enough systems the order parameter lines intersect. This suggests that the considered transition is of the first-order. Additional confirmation of this conclusion is given in figure 9(b), where we show the dependence of the maximum susceptibility $\chi_{corr}(L)$ on the system size. The slope (2.04) of this straight line is characteristic of first-order transitions (cf equation (18)).

5. Conclusions

We have used the hyper-parallel tempering Monte Carlo method and multiple-histogram techniques to study phase transitions of heterogeneous dimers on a three-dimensional simple cubic lattice. This model is closely related to the Blume–Capel model (see section 2), which is a generic model to qualitatively describe the phase behaviour of various systems, including binary mixtures (see section 1). The phase diagrams have been estimated for the selected sets of system parameters (u_{AA}, u_{BB}, u_{AB}). We have shown that the relative strength of interactions between different segments strongly affects the topology of the phase diagrams. We have found that depending upon the relation between energies two ordered structures may be formed, i.e. the AF phase and the SAF structure. The estimated phase diagrams include many interesting features, such as triple points, tricritical points, critical end-points, vapour–liquid coexistence, coexistence between a disordered and ordered liquid of the SAF type and the λ-line corresponding to a continuous transition between the disordered and the ordered fluid.

We have determined the fixed point cumulants for homogeneous dimers ($U_m^* = 0.47$), for symmetrical dimers ($u_{AA} = u_{BB} = -1$, $u_{AB} = 0.25$ $U_m^* = 0.47$) and the suitable critical parameters. These systems belong to the universality class of the three-dimensional Ising model.

We have studied systems with $u_{AB} = u_{BB} = -1$ and u_{AA} between -1 and 1. For $u_{AA} = 1$ the fixed point value of the cumulant was found to be $U_m^* \approx 0.36$. This value corresponds to the universality class of the tricritical Ising model. However, for $u_{AA} = 0.5$ and 0 the application of the cumulant crossing method requires application of much larger systems to achieve the required high accuracy.

In summary, it is quite clear that the choice of interactions between particular segments of heterogeneous dimers affects

their phase transitions in the three-dimensional case as well. The picture of phase behaviour of dimers is much more complicated than previously supposed.

Acknowledgments

This study was supported by the European Community under the grant MTKD-CT-2004-509249. One of us (WR) wants to acknowledge support from the Alexander von Humboldt Foundation.

References

[1] Hemmer P C and Stell G 1970 *Phys. Rev. Lett.* **24** 1284
[2] Binder K and Landau D P 1980 *Phys. Rev.* B **21** 1941
[3] Binder K, Kinzel W and Landau D P 1982 *Surf. Sci.* **117** 232
[4] Poland D 1999 *Phys. Rev.* E **59** 1523
[5] Groh B and Dietrich S 1994 *Phys. Rev. Lett.* **72** 2422
[6] Hemmer P C and Imbro D 1977 *Phys. Rev.* A **16** 380
[7] Hall C K and Stell G 1973 *Phys. Rev.* A **7** 1973
[8] Stell G and Hemmer P C 1972 *J. Chem. Phys.* **56** 4274
[9] Zhang H and Widom M 1994 *Phys. Rev.* E **49** R3591
[10] Załuska M A and Turski L A 1990 *Phys. Rev.* A **41** 3066
[11] Oukouios A and Baus M 1998 *J. Chem. Phys.* **109** 6157
[12] Tavares J M, Telo da Gama M M, Teixeria P I C, Weis J J and Nijmeijer M J P 1995 *Phys. Rev.* E **52** 1915
[13] Oukouios A and Baus M 1997 *Phys. Rev.* E **55** 7242
[14] Wilding N B and Nielaba P 1996 *Phys. Rev.* E **53** 926
[15] Weiss J J, Nijmeijer M J P, Tavares J M and Telo da Gama M M 1997 *Phys. Rev.* E **55** 436
[16] Marx P, Nielaba P and Binder K 1993 *Phys. Rev.* B **47** 7788
[17] Wilding N B, Schmid F and Nielaba P 1998 *Phys. Rev.* E **58** 2201
[18] Ciach A and Stell G 2002 *Physica* A **306** 220
[19] Ciach A and Stell G 2004 *Phys. Rev.* E **70** 016114
[20] Fowler R H and Rushbrooke G S 1937 *Trans. Faraday Soc.* **33** 1272
[21] Flory P 1942 *J. Chem. Phys.* **10** 51
[22] Kasteleyn P W 1961 *Physica (Utrecht)* **27** 1209
[23] Kasteleyn P W 1963 *J. Math. Phys.* **4** 287
[24] Fisher M E 1961 *Phys. Rev.* **124** 1664
[25] Phares A J, Wunderlich F J, Curley J D and Grumbine D W 1993 *J. Phys. A: Math. Gen.* **26** 6847
[26] Wojciechowski K W 1992 *Phys. Rev.* B **46** 26
[27] Wojciechowski K W, Frenkel D and Branka A C 1991 *Phys. Rev. Lett.* **66** 3168
[28] Alet F, Jacobsen J L, Misguich G, Pasquier V, Mila F and Troyer M 2005 *Phys. Rev. Lett.* **94** 235702
[29] Alet F, Ikhlef Y, Jacobsen J L, Misguich G and Pasquier V 2006 *Phys. Rev.* E **74** 041124
[30] Ramirez-Pastor A J, Riccardo J L and Pereyra V D 1998 *Surf. Sci.* **411** 294
[31] Roma F, Ramirez-Pastor A J and Riccardo J L 2003 *Phys. Rev.* B **68** 205407
[32] Rżysko W and Borówko M 2002 *J. Chem. Phys.* **117** 4526
[33] Rżysko W and Borówko M 2002 *Surf. Sci.* **520** 151
[34] Rżysko W and Borówko M 2003 *Physica* A **326** 1
[35] Rżysko W and Borówko M 2006 *Surf. Sci.* **600** 890
[36] Rżysko W and Borówko M 2003 *Thin Solid Films* **425** 304
[37] Rżysko W, Patrykiejew A and Binder K 2005 *Phys. Rev.* B **72** 165416
[38] Rżysko W, Patrykiejew A and Binder K 2007 *Phys. Rev.* B **76** 195409
[39] Schmid F 2000 *Computational Methods in Surface and Colloid Science* (*Surfactant Series* vol 89) ed M Borówko (New York: Dekker) pp 631–82
[40] Schmicker D, Toennies J P, Vollmer R and Weiss J J 1991 *J. Chem. Phys.* **95** 9412
[41] Heidberg J, Kampshoff E and Suhren M 1991 *J. Chem. Phys.* **95** 9408
[42] Vu N T, Jakalian A and Jack D B 1997 *J. Chem. Phys.* **106** 2551
[43] Minot Ch, Van Hove M A and Biberian J P 1996 *Surf. Sci.* **346** 283
[44] Zecchina A and Scarano D 1986 *Surf. Sci.* **166** 347
[45] Blume M, Emery V J and Griffiths R B 1971 *Phys. Rev.* A **4** 1071
[46] Blume M 1996 *Phys. Rev.* **141** 517
[47] Capel H W 1966 *Physica (Amsterdam)* **32** 966
[48] Bruce A D and Wilding N B 1992 *Phys. Rev. Lett.* **68** 193
[49] Müller M and Wilding N B 1995 *Phys. Rev.* E **51** 2079
[50] Virnau P, Müler M, MacDowell L G and Binder K 2004 *J. Chem. Phys.* **121** 2169
[51] Frenkel D and Smit B 1996 *Understanding Molecular Simulations from Algorithms to Applications* (San Diego, CA: Academic)
[52] Binder K (ed) 1978 *Monte Carlo Methods in Statistical Physics* (*Springer Topics in Current Physics* vol 7) (Berlin: Springer)
[53] Landau D P and Binder K 2000 *A Guide to Monte Carlo Simulation in Statistical Physics* (Cambridge: Cambridge University Press)
[54] Yan Q and de Pablo J J 1999 *J. Chem. Phys.* **111** 9509
[55] de Pablo J J, Yan Q and Escobedo F A 1999 *Annu. Rev. Phys. Chem.* **50** 377
[56] Ferrenberg A M and Swendsen R H 1988 *Phys. Rev. Lett.* **61** 2635
[57] Binder K 1981 *Phys. Rev. Lett.* **47** 693
[58] Binder K and Landau D P 1984 *Phys. Rev.* B **30** 1477
[59] Challa M S S, Landau D P and Binder K 1986 *Phys. Rev.* B **34** 1841
[60] Vollmayr K, Reger J D, Scheucher M and Binder K 1993 *Z. Phys.* B **91** 113
[61] Ferrenberg A M and Landau D P 1991 *Phys. Rev.* B **44** 5081
[62] Deserno M 1997 *Phys. Rev.* E **56** 5204
[63] Deng Y and Blöte H W J 2004 *Phys. Rev.* E **70** 046111
[64] Kutlu B, Özkan A, Seferoglu N, Solak A and Binal B 2005 *Int. J. Mod. Phys.* C **16** 933
[65] Tsypin M M and Blöte H W J 2000 *Phys. Rev.* E **62** 73
[66] Bausch R 1972 *Z. Phys.* **254** 81